04,05

The effect of a weak pulsed magnetic field on the ionic conductivity of the superionic conductor $Pb_{0.67}Cd_{0.33}F_2$

© N.I. Sorokin, V.M. Kanevskii

Institute of Crystallography named after A.V. Shubnikov FSRC „Crystallography and Photonics“ RAS, Moscow, Russia

E-mail: nsorokin1@yandex.ru

Received April 27, 2023
Revised July 7, 2023
Accepted July 21, 2023

A magnetoconductometric effect was found under pulsed magnetic action ($B = 0.1-1$ T) on a single crystal of the superionic conductor $Pb_{0.67}Cd_{0.33}F_2$ (cubic symmetry, space group $Fm\bar{3}m$, unit cell parameter $a = 5.7575$ Å). The static electrical conductivity σ_{dc} was determined from impedance spectra in the frequency range $(5-5) \cdot 10^5$ Hz. In the absence of magnetic influence ($B = 0$) the ionic conductivity of a superionic crystal is $\sigma_{dc} = 1.4 \cdot 10^{-4}$ S/cm. When applying a magnetic field ($B = (0.1-1)$ T) it increases, reaching $\sigma_{dc} = 9.5 \cdot 10^{-4}$ S/cm and $\sigma_{dc}(B)/\sigma_{dc}(0) = 6.8$ at $B = 1$ T. The nature of the magnetoconductometric effect in the superionic $Pb_{0.67}Cd_{0.33}F_2$ is discussed in connection with the features its atomic structure.

Keywords: superionic conductivity, magnetoconductometric effect, fluorides, fluorite-type structure.

DOI: 10.61011/PSS.2023.09.57111.72

1. Introduction

Superionic conductors having abnormally high conductivity in solid state are functional materials of great interest in solid-state physics and electrochemistry. They are widely used as solid-state electrolytes in advanced development of galvanic cells, gas and liquid sensors.

An effective method for control of ionic crystal properties includes rearrangement of actual crystal structures under various external impacts, including the application of magnetic field. Weak pulsed magnetic fields ($B < 1$ T) (PMF) are known to impact [1–4] the defect structure and physical properties of non-magnetic ionic crystals by changing their energy state. It is important to study the PMF impact on the conductivity of superionic conductors.

Low-temperature superionic $Pb_{0.67}Cd_{0.33}F_2$ conductor with high unipolar fluorine-ionic conductivity was chosen as a model crystal [5–7]. Its electronic conductivity may be ignored (it is not higher than 0.01% of the total conductivity) [5,8]. It is an isovalent solid solution with the fluorite structure (CaF_2 type, space group $Fm\bar{3}m$) and composition corresponding to the minimum on the liquidus curve in PbF_2-CdF_2 system. Coordinates of the minimum are $t = 745 \pm 5°C$, 67 ± 2 mol.% PbF_2 and 33 ± 2 mol.% CdF_2 [7]. Congruent nature of melting of $Pb_{0.67}Cd_{0.33}F_2$ solid solution offers the opportunity of growing crystals with homogeneous composition from the melt [7,9,10].

Ionic conductivity of $Pb_{0.67}Cd_{0.33}F_2$ single-crystals was studied in [6,7,11,12], it is equal to $\sigma_{dc} \approx 10^{-4}$ S/cm at room temperature. Anionic conductivity of $Pb_{0.67}Cd_{0.33}F_2$ is caused by the anti-Frenkel defects with isomorphous substitutions of Pb^{2+} cations on Cd^{2+} [12–14]. High ionic conductivity in combination with low melting temperature allows to address fluorite $Pb_{0.67}Cd_{0.33}F_2$ solid solution as a promising parent matrix for production of new fluorine solid-state electrolytes for galvanic cells operated at room temperature [15,16].

The objective of this study was to investigate the influence of pulsed magnetic field on superionic conductivity $Pb_{0.67}Cd_{0.33}F_2$.

2. Experiment and discussion of results

$Pb_{1-x}Cd_xF_2$ solid solution single-crystals with $x = 0.33$ were produced from the melt by the vertical Bridgman directional solidification in fluorinating atmosphere (polytetrafluorethylene pyrolysis products). The crystal growth technique is described in detail in [7,10]. The structure of the grown crystal is classified as cubic crystal system (space group $Fm\bar{3}m$, formula units per lattice cell $Q = 4$). The lattice cell constant is equal to $a = 5.7575$ Å (Rigaku MiniFlex 600 powder diffractometer, radiation CuK_α).

The test sample was prepared in the form of a cylinder 8 mm in diameter and 1.2 mm in thickness. The sample was not subjected to crystal-lattice orientation, because the $Pb_{0.67}Cd_{0.33}F_2$ crystal structure is classified as cubic symmetry and there is now conductivity anisotropy in it.

Static DC conductivity σ_{dc} of the crystal was measured by the impedance spectroscopy [17,18]. Leitsilber silver paste was used as conducting contacts and applied to the work (end) surfaces of the cylindrical sample. Complex impedance $Z^*(\omega)$ ($Z^* = Z' + iZ''$, real component $Z' = |Z| \cos\varphi$, imaginary component $Z'' = |Z| \sin\varphi$, $|Z|$ — scalar impedance, φ — phase angle between voltage and current, ω — angular frequency) of the electrochemical $Ag|Pb_{0.67}Cd_{0.33}F_2|Ag$ system was mea-

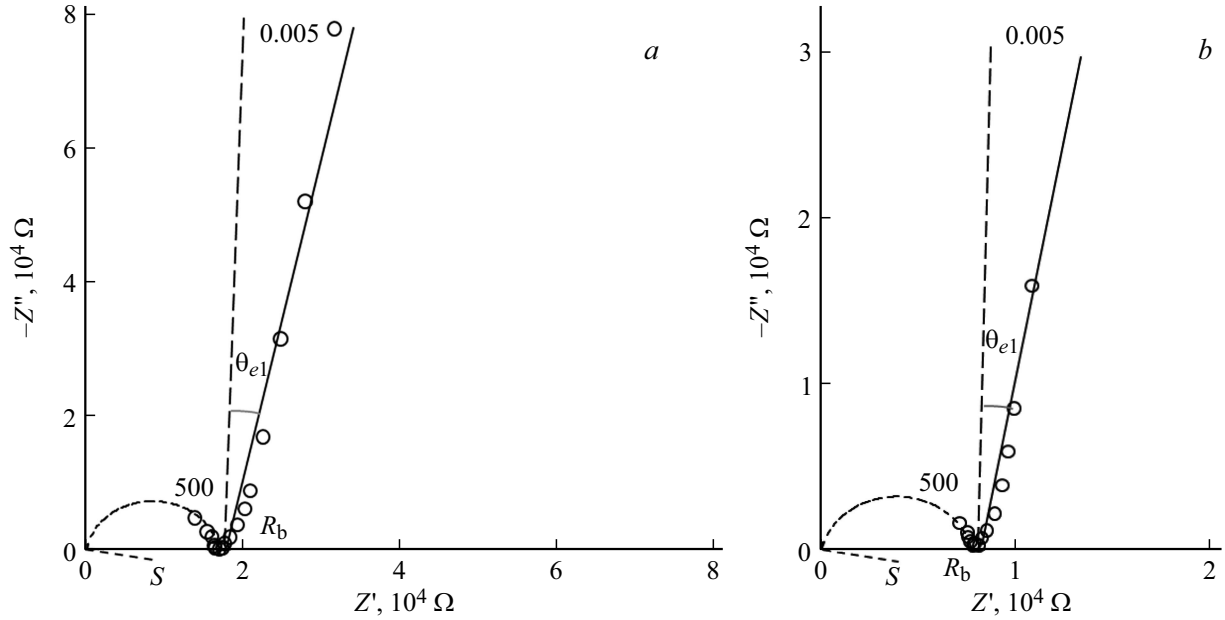

Figure 1. Impedance loci $Z^*(\omega) = Z' + iZ''$ of Ag|$Pb_{0.67}Cd_{0.33}F_2$|Ag system: *a*) without magnetic action and *b*) with enabled magnetic action ($B = 0.4$ T, $t = 60$ min). Calculated R_b and θ_{el} values are listed in the Table. Here, $B = 0$ is the electric field frequency in kHz. Circles *S* are drawn approximately.

sured at $(5-5) \cdot 10^5$ Hz and $(1-10^7)$ Ω (Tesla BM-507 impedancemeter), in vacuum 1 Pa. Relative measurement error $Z^*(\omega)$ was 5%. The impedance measurement procedure is described in detail in [19–21]. Impedance spectra parameters were calculated by non-linear square method using FIRDAC software package [22].

The crystal was exposed to PMF by means of periodic capacitor discharge through a solenoid. Pulse repetition rate, length and amplitude in the inductor were equal to 12 Hz, 12 ms and $B = (0.1-1)$ T, respectively. Magnetic induction vector was parallel to the sample work surfaces.

Figures 1 and 2 show the impedance loci in the complex plane $Z^* = Z' + iZ''$ (Nyquist diagrams), frequency dependences of scalar impedance $|Z|$ and phase angle φ for $Pb_{0.67}Cd_{0.33}F_2$ single-crystal with silver electrodes without magnetic action and, as an example, in one of the states with enabled magnetic action.

The Nyquist diagrams obviously have the same form. Complex impedance of $Z^*(\omega)$ system consists of two components: volumetric $Z_b^*(\omega)$ at high frequencies and electrode $Z_{el}^*(\omega)$ at low frequencies. In the operating frequency range, the impedance loci generally contain the impedance electrode component $Z_{el}^*(\omega)$ in the form of deviations from the vertical position of the straight line intersecting the resistance axis Z' in point R_b (with phase angle between voltage and current $\varphi = 0°$).

Volumetric impedance sections $Z_b^*(\omega)$ are negligible. With decreasing temperature, the resistance will grow, therefore the impedance locus branch $Z_b^*(\omega)$ responsible for the crystal dielectric properties will become more apparent. It can be assumed that the volumetric impedance sections $Z_b^*(\omega)$ observed in Figure 1 probably constitute a minor portion of half-circles extrapolated to the origin of coordinates whose center in below the Z' axis of resistances. Such half-circles have been observed before in the volumetric impedance loci $Z_b^*(\omega)$ for superionic fluorine $M_{1-x}R_xF_{2+x}$ and $Na_{0.5-x}R_xF_{2+x}$ conducor single-crystals (M = Ca, Sr, Ba, Pb; R is a rare earth element) with the fluorite structure [23–26].

Complex impedance loci for $Pb_{0.67}Cd_{0.33}F_2$ single-crystal and other superionic fluorines [23–26] with inert electrodes correspond to the equivalent AC circuit shown in Figure 3. Here, the resistor R_b defines the volumetric resistance of the crystal directly associated with the ionic conductivity, and constant phase elements with constant phase angle $P_b(\omega)$ and $P_{el}(\omega)$ (CP elements [17,18]) simulate the polarization processes within the crystal and at the electrode/crystal interface. CP element admittance $P(\omega)$ is equal to $Y_P^* = 1/Z_P^* = Y_0(i\omega)^n$, $0 \le n \le 1$. In electrical processes at $n = 1$, CP elements $P_b(\omega)$ and $P_{el}(\omega)$ are transformed into the geometrical capacity C_g and double-layer capacity C_{dl}, respectively ($Z_C^* = 1/i\omega C$). The use of capacities C_g and C_{dl} in the equivalent diagram is indicative of the electrical process uniformity, while the CP elements $P_b(\omega)$ and $P_{el}(\omega)$ exhibiting capacitive reactance ($0.7 < n < 1$) correspond to non-uniform processes with characteristic frequency (or time) distribution.

At low frequencies ($f < 10^3$ Hz, Figure 2), the effect of the CP element $P_b(\omega)$ may be ignored (its impedance is very high compared with R_b), therefore for the electrode impedance $Z_{el}^*(\omega)$, a more simple equivalent diagram will be obtained, which consists of resistance R_b and constant phase element $P_{el}(\omega)$ connected in series.

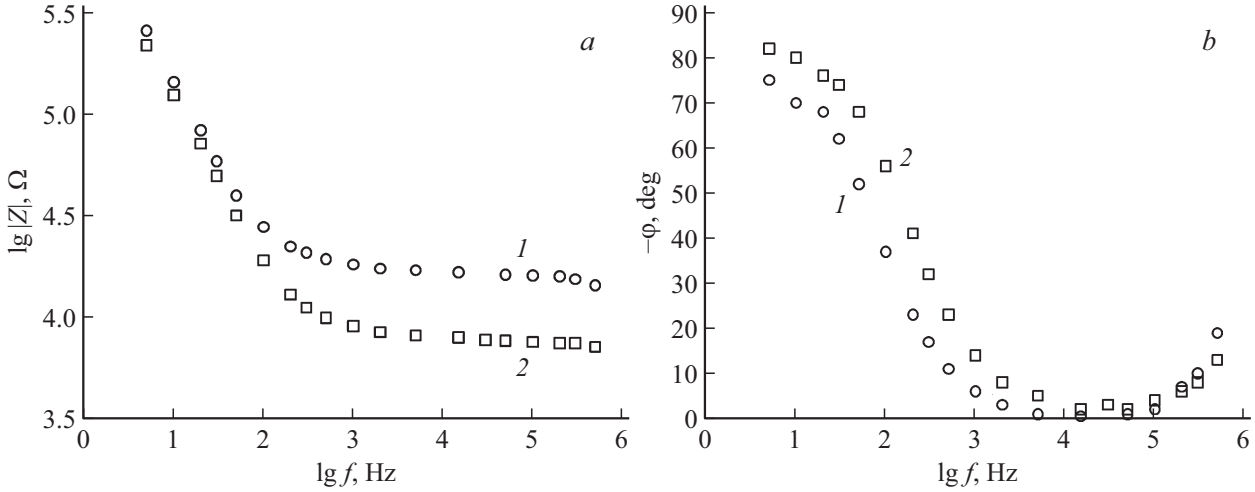

Figure 2. Comparison of frequency dependences *a*) scalar impedance $|Z|$ and *b*) phase angle φ between voltage and current for $Ag|Pb_{0.67}Cd_{0.33}F_2|Ag$ system without magnetic action (curve *1*) and with enables magnetic action ($B = 0.4$ T, $t = 60$ min) (curve *2*).

In this case, the electrode admittance $Y^*_{el}(\omega)$ may be written as

$$Y^*_{el} = G_b/[1 + (i\omega/\omega_{el})^{n_{el}}], \quad (1)$$

where $G_b = 1/R_b$. Here, the frequency ω_b corresponds to the peak of $Y''_{el}(\omega)$:

$$dY''_{el}/d\omega = 0 \quad \text{by} \quad \omega_{el} = [G_b/Y_{0,el}]^{1/n_{el}}. \quad (2)$$

The Table lists the electrode impedance and angles of depression with/without magnetic action calculated by the least-square method (LSM). θ_{el} ($\theta_{el} = \pi(1 - n_{el})/2$)

As shown in the Table, CP element properties $P_{el}(\omega)$, when exposed to the magnetic field, remain almost the same, while the volumetric resistance R_b was 2.2 times lower.

For the experimental values of n_{el}, with neglecting the deviation rom the ideal capacity behavior ($n_{dl} = 1$), $Y_{0,el}$ values represent volumetric data. Then the capacity of $Ag|Pb_{0.67}Cd_{0.33}F_2$ phase interface is equal to

$$C_{dl} = Y_{0,el}/S = 4 \cdot 10^{-7}\ \text{F/cm}^2. \quad (3)$$

The resulting value of C_{dl} for $Pb_{0.67}Cd_{0.33}F_2$ crystal agree closely with similar properties of crystalline ($Ca_{1-x}R_xF_{2+x}$, $Na_{0.5-x}R_{0.5+x}F_{2+2x}$) and amorphous

Electrode impedance of $Ag|Pb_{0.67}Cd_{0.33}F_2|Ag$ system calculated by the LSM method

Description	without magnetic action	With enabled magnetic action ($B = 0.4$ T, $t = 60$ min)
R_b, Ω	$(1.7 \pm 0.1) \cdot 10^4$	$(7.7 \pm 0.4) \cdot 10^3$
$Y_{0,el}$, $S\,(Hz)^{-n}_{el}$	$(2.0 \pm 0.1) \cdot 10^{-7}$	$(2.0 \pm 0.1) \cdot 10^{-7}$
n_{el}	0.87 ± 0.01	0.89 ± 0.01
θ_{el}, deg	12 ± 1	10 ± 1

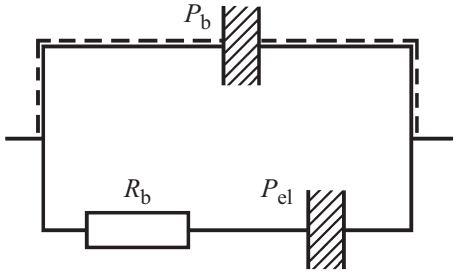

Figure 3. Equivalent circuit diagram simulating the impedance of $Ag|Pb_{0.67}Cd_{0.33}F_2|Ag$ system. Designation of the diagram elements is provided in the text.

($40GaF_3-40BaF_2-20YbF_3$) fluorine-ionic conductors with inert (blocking) electrodes [26–28].

Capacitive reactance of the electrode element $P_{el}(\omega)$ ($n_{el} \approx 0.9$) is indicative of the ionic nature of the electrotransport in the test crystal. In superionic $Pb_{0.67}Cd_{0.33}F_2$ conductor, ionic transport is provided by mobile F^- ions. This is directly shown by the nuclear magnetic resonance examination ^{19}F [14,29], where high diffusion of F^- ions was detected in $Pb_{0.67}Cd_{0.33}F_2$ solid solution. Theoretical calculations by the molecular dynamics and quantum chemistry methods [13,30] confirm the fluorine-ionic mechanism of conductivity in this crystal.

Volumetric impedance $Z^*_b(\omega)$ observed at high frequencies ($f > 10^5$ Hz, Figure 2), taking into account the impedance data for superionic fluorine crystals with the fluorite structure [23–26], is probably a minor portion of the half-circle extrapolated to the origin of coordinates. However, for accurate determination of the volumetric impedance $Z^*_b(\omega)$, it is necessary to increase the volumetric resistance R_b of the crystal by decreasing the temperature.

As a result, when the magnetic field is applied, impedance measurements ensure reliable determination of

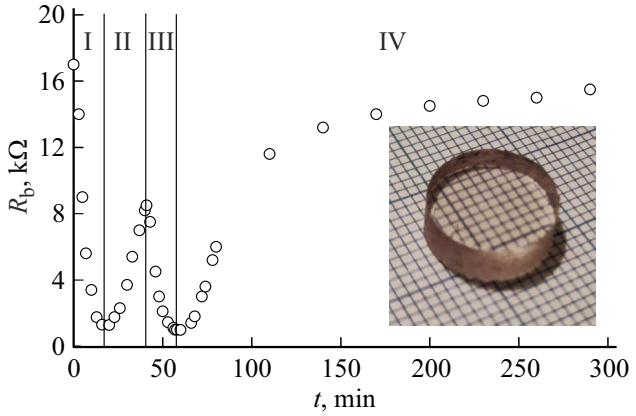

Figure 4. Kinetics of the volumetric resistance $R_b(t)$ ($R_b \propto \sigma_{dc}^{-1}$) for superionic $Pb_{0.67}Cd_{0.33}F_2$ in four PMF enabling–disabling modes: I — mode 1 at $B = 1$ T, II — mode 2 at $B = 0$, III — mode 3 at $B = 1$ T and IV — mode 4 at $B = 0$. The detail on the graph paper shows the central part of the grown crystalline ingot 8 mm in diameter with optic quality, from which the sample was made.

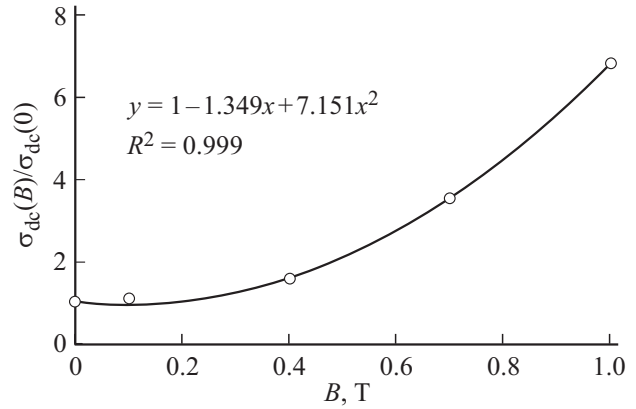

Figure 5. $\sigma_{dc}(B)/\sigma_{dc}(0)$ vs. magnetic action amplitude B for superionic $Pb_{0.67}Cd_{0.33}F_2$ (R is the correlation coefficient).

the volumetric resistance R_b of the single-crystal directly associated with the translation fluorine ionic transport in the lattice and investigation of the magnetic field effect on the ionic conductivity of the superionic conductor.

Figure 4 shows the volumetric resistance variation of the superionic crystal R_b in four modes with successive enabling and disabling of PMF with amplitude $B = 1$ T. It can be seen that in the sections with applied PMF (modes *1* and *3*), R_b decreases, and when the magnetic action id disabled (modes *2* and *4*), it relaxes to the initial value.

Conductivity σ_{dc} was calculated as follows

$$\sigma_{dc} = h/(SR_b), \tag{4}$$

where the geometrical factor $h/S = 2.38\,\text{cm}^{-1}$, h is the crystal thickness and S is the electrode area. Without magnetic action ($B = 0$), ionic conductivity of the superionic crystal is equal to $\sigma_{dc} = 1.4 \cdot 10^{-4}$ S/cm. When the magnetic field is applied, σ_{dc} increases reaching $9.5 \cdot 10^{-4}$ S/cm at $B = 1$ T, while the conductivity increase is $\sigma_{dc}(B)/\sigma_{dc}(0) = 6.8$ times. After PMF exposure, ionic conductivity of the crystal decreases to the initial value.

Thus, the high-conducting $Pb_{0.67}Cd_{0.33}F_2$ crystal case study showed that the magnetic field action results in relaxation changes of ionic conductivity of the superionic conductor or in magnetic-conductometric effect.

For $B = 0.1$, 0.4 and 0.7 T cases, the ionic conductivity kinetics with enabled ($B \neq 0$) and disabled ($B = 0$) magnetic field flow in the same way, but the effect is weaker. Figure 5 shows magnetically induced changes of ionic conductivity of $Pb_{0.67}Cd_{0.33}F_2$ single-crystal depending on the PMF amplitude. With decreasing magnetic action B, the conductivity increase effect decreases and can be described in the first approximation by quadratic dependence.

The nature of magnetic-conductometric effect in superionic $Pb_{0.67}Cd_{0.33}F_2$ is associated with the features of atomic configuration. DC conductivity σ_{dc} of crystals is a microscopic physical quantity combining microscopic properties of charge carriers. In superionic conductors, it depends on mobility μ_{mob} and concentration n_{mob} of the conductivity ions ($\sigma_{dc} \propto n_{mob}\mu_{mob}$). Mobility of ionic charge carriers characterizes microscopic movement of the conductivity ions in the crystal lattice relative to the external electric field action.

$Pb_{0.67}Cd_{0.33}F_2$ fluorite crystal has rigid cation (Pb^{2+}, Cd^{2+}) and mobile anion (F^-) sublattices. Magnetic field impacts the energetic state of the mobile fluorine-ionic sublattice, and the nature of Coulomb interaction of anion charge carriers with cation lattice varies. Superionic conductor exposure to PMF results in increasing mobility of anion defects, which manifests itself in increasing anion conductivity σ_{dc}.

It can be assumed that the change of the energy state of the mobile fluorine-ionic sublattice may be associated with magnetoplastic effect [3,31], that has been observed earlier in ionic crystals (LiF, NaCl) in superlow magnetic fields. According to [3,31], the magnetoplastic effect in non-magnetic crystals is caused by strain softening of the structure due to dislocation migration in crystals when they are held in magnetic field (without mechanical load). The softening effect of magnetic field on ionic crystals is manifested in decreasing microhardness, strain hardening rate and yield strength. In [32], it was found that magnetic field also affects semiconductor photoconductivity, amorphous alloy viscosity and chemical reaction rate. However, to study magnetic-conductometric effect in superionic crystals, further investigations are required.

3. Conclusion

By way of example of $Pb_{0.67}Cd_{0.33}F_2$ conductor, magnetic-conductometric effect was detected — ionic conductivity response of the non-magnetic crystal to the external magnetic field. Ionic conductivity kinetics in superionic

$Pb_{0.67}Cd_{0.33}F_2$ crystal was studied during and after exposure to PMF with amplitude $B = (0.1-1)$ T. It has been found that, when the magnetic field is applied, the ionic conductivity increases and achieves $\sigma_{dc}(B)/\sigma_{dc}(0) = 6.8$ at $B = 1$ T, and, when the magnetic field is disabled, the ionic conductivity relaxes to the initial value. The nature of the magnetic-conductometric effect is associated with the features of atomic configuration of superionic $Pb_{0.67}Cd_{0.33}F_2$ having a disordered sublattice of mobile fluorine ions. In the magnetic field, the fluorine-ionic conductivity σ_{dc} increases as a result of increasing mobility of anionic defects.

Acknowledgments

The authors are grateful to I.I. Buchinskaya for the crystal provided for the study.

Funding

The study was carried out under the state assignment of FSRC„Crystallography and Photonics“ RAS.

References

[1] G.I. Distler, V.M. Kanevsky, V.V. Moskvin, S.N. Postnikov, L.A. Ryabinin, V.P. Sidorov, G.D. Sidiriv, G.D. Shnyrev. DAN SSSR **268**, *3*, 591 (1983). (in Russian).
[2] I.S. Volchkov, V.M. Kanevskii, M.D. Pavlyuk. JETP Lett. **107**, *4*, 269 (2018).
[3] V.I. Alshits, E.V. Darinskaya, A.A. Urusovskaya, E.S. Goryunov. FTT **29**, *2*, 467 (1987). (in Russian).
[4] M.N. Levin, V.V. Postnikov, M.Yu. Palagin, A.M. Kostsov. Phys. Solid State **45**, *3*, 542 (2003).
[5] I.V. Murin, S.V. Tchernov. Izv. AN SSSR. (in Russian) Neorgan. materialy **18**, *1*, 168 (1982). (in Russian).
[6] N.I. Sorokin. Phys. Solid State **57**, *7*, 1352 (2015).
[7] N.I. Sorokin, I.I. Buchinskaya, B.P. Sobolev. Zhurn. neorgan. khimii **37**, *2653*, 1992 (2021). (in Russian).
[8] I. Kosacki. Appl. Phys. A **49**, *4*, 413 (1989).
[9] P.P. Fedorov, I.I. Buchinskaya, E.V. Chernova. Crystallogr. Reps **61**, *3*, 512 (2016).
[10] I. Kosacki, E. Dynowska. J. Cryst. Growth **50**, *2*, 575 (1980).
[11] N.I. Sorokin, I.I. Buchinskaya. Crystallogr. Reps **67**, *6*, 958 (2022).
[12] V. Trnovcová, P.P. Fedorov, M. Ozvoldova, I.I. Buchinskaya, E.A. Zhurova. J. Optoelectron. Adv. Mater. **5**, *3*, 627 (2003).
[13] I.V. Murin, E.M. Piotrovskaya, E.N. Brodskaya. Inorg. Mater. **39**, *3*, 291 (2003).
[14] V.M. Buznik, A.A. Sukhovsky, V.A. Vopilov, V.M. Mastikhin, P.P. Fedorov, I.I. Buchinskaya, B.P. Sobolev. Zhurn. neorgan. khimii, **42**, *12*, 2092 (1997). (in Russian).
[15] G. Karkera, M. Anji Reddy, M. Fichtner. J. Power Sources **481**, 228877 (2021).
[16] M. Anji Reddy, M. Fichtner. J. Mater. Chem. **21**, *43*, 17059 (2011).
[17] A.K. Ivanov-Shits, I.V. Murin. Ionika tverdogo tela. Izd-vo SPb un-ta, SPb (2000). T. 1. 616 p. (in Russian).
[18] E. Barsoukov, J.R. Macdonald. Impedance Spectroscopy: Theory, Experiment and Applications. Wiley, N.Y. (2005). 606 p.
[19] N.I. Sorokin, Yu.V. Pisarevskii, V.V. Grebenev, V.A. Lomonov. Phys. Solid State **62**, *3*, 436 (2020).
[20] I.I. Buchinskaya, D.N. Karimov, N.I. Sorokin. Crystals **11**, *6*, 629 (2021).
[21] N.I. Sorokin, D.N. Karimov, I.I. Buchinskaya. Russ. J. Electrochem. **57**, *8*, 833 (2021).
[22] J.P. Dygas. PhD Thesis. Northwestern University, Evanston (1986).
[23] N.I. Sorokin, B.P. Sobolev. Russ. J. Electrochem. **45**, *11*, 1296 (2009).
[24] N.I. Sorokin. Russ. J. Electrochem. **41**, *8*, 896 (2005).
[25] N.I. Sorokin, M.V. Fominykh, E.A. Krivandina, Z.I. Zhmurova, B.P. Sobolev. Crystallogr. Reps **41**, *2*, 292 (1996).
[26] A.K. Ivanov-Shits, N.I. Sorokin. Solid State Ionics **36**, *1–2*, 7 (1989).
[27] N.I. Sorokin, A.K. Ivanov-Shits, L.L. Vistin, B.P. Sobolev. Kristallografiya **37**, *421*, 1992 (1983). (in Russian).
[28] N.I. Sorokin, P.P. Fedorov, B.P. Sobolev. Kristallografiya **39**, *1*, 119 (1994). (in Russian).
[29] A.I. Matsulev, Yu.N. Ivanov, A.I. Livshits, V.M. Buznik, P.P. Fedorov, I.I. Buchinskaya, B.P. Sobolev. Zhurn. neorgan. khimii **45**, *296*, (2000). (in Russian).
[30] A.V. Petrov, M.S. Salamatov, A.K. Ivanov-Schitz, I.V. Murin. Crystallogr. Reps **64**, *6*, 932 (2019).
[31] V.I. Alshits, E.V. Darinskaya, M.V. Koldaeva, E.A. Petrzhik. Crystallogr. Reps **48**, *5*, 768 (2003).
[32] Yu.I. Golovin. Phys. Solid State **46**, *5*, 789 (2004).

Translated by E.Ilyinskaya